Analytical and Bioanalytical Chemistry
https://doi.org/10.1007/s00216-018-0970-5

RESEARCH PAPER

Novel electrochemical aptasensor for ultrasensitive detection of sulfadimidine based on covalently linked multi-walled carbon nanotubes and in situ synthesized gold nanoparticle composites

Baoshan He[1] · Gengan Du[1]

Received: 21 November 2017 / Revised: 1 January 2018 / Accepted: 17 February 2018

Abstract
In the current study, a sensitive electrochemical sensing strategy based on aptamer (APT) for detection of sulfadimidine (SM_2) was developed. A bare gold electrode (AuE) was first modified with 2-aminoethanethiol (2-AET) through self-assembly, used as linker for the subsequent immobilization of multi-walled carbon nanotubes and gold nanoparticle composites (MWCNTs/AuNPs). Then, the thiolated APT was assembled onto the electrode via sulfur-gold affinity. When SM_2 existed, the APT combined with SM_2 and formed a complex structure. The specific binding of SM_2 and APT increased the impedance, leading to hard electron transfer between the electrode surface and the redox probe $[Fe(CN)_6]^{3-/4-}$ and producing a significant reduction of the signal. The SM_2 concentration could be reflected by the current difference of the peak currents before and after target binding. Under optimized conditions, the linear dynamic range is from 0.1 to 50 ng mL^{-1}, with a detection limit of 0.055 ng mL^{-1}. The sensor exhibited desirable selectivity against other sulfonamides and performs successfully when analyzing SM_2 in pork samples.

Keywords Sulfadimidine · Electrochemical aptasensor · 2-Aminoethanethiol · Multi-walled carbon nanotubes · Gold nanoparticles

Introduction

Sulfonamide antibiotics (SAs), a series of synthetic antimicrobials containing a $–SO_2NH_2–$ group, have been widely used as veterinary drugs to inhibit bacterial growth and treat the infections in livestock production. However, indiscriminate use of SAs in animal breeding can result in unacceptably high residues in foods [1]. The unwanted residues in animal feed may induce hypersensitive allergic reactions and drug resistance problems in humans. Some SAs are even potentially carcinogenic [2, 3]. Given the food safety and public health concerns, many countries have been legally established the maximum residue limits (MRLs). According to European Union regulations, the MRL of SAs in foods from animal origin is 100 ng g^{-1} [4]. Therefore, it is necessary to establish a rapid and simple analytical method to determine the SA residues in various samples.

So far, methods such as liquid chromatography/tandem mass spectrometry (LC-MS/MS) [5–8], high-performance liquid chromatography (HPLC) [9–11], capillary electrophoresis [12, 13], enzyme-linked immune assay [14, 15], and biosensor-based assays [16, 17] have been developed to analyze SA residues. Whereas these techniques have achieved satisfactory results, some of them are generally cumbersome and slow, and thus, the development of a real-time means for such targets remains a compelling goal.

Recently, the aptasensors have been studied widely because of their unique advantages. Aptamer (APT) is a single-stranded DNA or RNA ligand artificially selected for various targets including small molecules, proteins, and cells with specificity and high affinity. Compared with antibodies as recognition elements, APT is such easier in synthesize and more versatility in labeling, immobilization, and signaling [18–20]. Therefore, numerous reports have studied on aptasensors utilizing various signal transducers, such as

✉ Baoshan He
hebaoshan@126.com

[1] School of Food Science and Technology, Henan University of Technology, Lianhua Road 100#, Zhengzhou, Henan 450001, China

Published online: 03 March 2018

fluorescent [21], colorimetric [22, 23], and electrochemical systems [24, 25]. Among these methods, electrochemical detection have attracted lots of attention because it is rapid and cost-effective. More and more researchers focus on the use of electrochemical aptasensor for SA detection.

Although APT is the promising specificity recognition element, one major drawback of APT is a rather poor detection limit that was caused by the relatively low association constants with small molecules. Because of this defect, the high sensitivity required in determination of small molecules based on APT is hard to achieve by simple "direct" binding. Hence, many works have been focused on using nanomaterial modification to improve the response signal.

Multi-walled carbon nanotubes (MWCNTs) have received particular attention due to their rich nanoporous, their layered, and hollow structures [26], and their unique mechanical and electrical properties [27, 28]. MWCNTs are widely served as a perfect electrode-modifying material because of their high specific surface area and excellent electrical performance. MWCNTs functionalized with noble nanoparticles are also considered as immobilization matrices with synergistic purpose. Gold nanoparticles (AuNPs) are one of the highly studied nanoparticles in noble nanoparticles, owing to the superior merits such as electrocatalytic ability, excellent conductivity, and biocompatibility [29, 30]. The composites of MWCNTs and AuNPs have been shown to be an effective approach to enhance the properties of aptasensors [31–33].

In this study, we have developed electrochemical aptasensor based on MWCNTs/AuNPs/AuE for the quantitative detection of sulfadimidine (SM_2; Scheme 1). For this purpose, an AuE is first modified with 2-aminoethanethiol (2-AET) through self-assembly to immobilize the MWCNT/AuNP nanocomposites via the formation of amidic bonds between the aminic functionalities of the 2-AET and the carboxyl groups of MWCNTs (the MWCNTs are functionalized with carboxyl groups by strong mixed acid pretreatment). Then, thiolated APT was assembled onto the electrode via sulfur-gold affinity. Upon SM_2 binding, electron transfer is inhibited, probably due to the formation of APT and SM_2 can block the diffusion of $[Fe(CN)_6]^{3-/4-}$ towards the surface of working electrode, producing a significant reduction of the signal. Differential pulse voltammetry (DPV) was investigated for the reading of the assay.

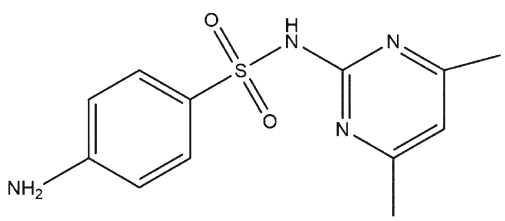

Scheme 1 Chemical structure of sulfadimidine

For all we know, there is rarely previous report on electrochemical aptasensor for SM_2 detection based on the MWCNTs/AuNPs/AuE. With this system, the SM_2 could be specifically detected, and a wide linear dynamic range as well as a low detection limit could be achieved. Meanwhile, the optimal conditions and other performance characteristics of the detection system were also investigated: selectivity, reproducibility, and stability, for example. Furthermore, the constructed electrode could be performed successfully to detect SM_2 in pork samples.

Experimental

Reagents and materials

Thiol-terminated DNA oligonucleotides were received from Sangon Biotech Co., Ltd. (Shanghai, China). The sequences of employed single oligonucleotides are as follows: 5′SH-TTA GCT TAT GCG TTG GCC GGG ATA AGG ATC CAG CCG TTG TAG ATT TGC GTT CTA ACT CTC-3′ (DNA). MWCNT was purchased from Beijing Gaoke Technology Material Co., Ltd. (Beijing, China). SM_2 and chloroauric acid ($HAuCl_4$) were ordered from Aladdin Industrial Co., Ltd. (Shanghai, China). 6-Mercapto-1-hexanol (MCH), N-hydroxysuccinimide (NHS), N-(3-dimethylaminopropyl)-N′-ethylcarbodiimide (EDC), and 2-AET were received from Shanghai Yuanye Bio-Technology Co., Ltd. (Shanghai, China). Tris-HCl (10 mM, 1 mM EDTA, pH 7.4) was used as a solvent of APT. Phosphate-buffered solution (PBS; 20 mM, pH 7.4) consisted of Na_2HPO_4, NaH_2PO_4, and NaCl solutions. All other chemicals used were of analytical grade.

Apparatus

Electrochemical tests were carried out on the CHI660E electrochemical workstation (Shanghai Chenhua Instrument Corporation, China) with a conventional three-electrode cell that contained an AuE or modified AuE as working electrode, an Ag/AgCl as reference electrode, and a platinum wire as counter electrode. Fourier transform infrared spectroscopy (FTIR) and transmission electron microscopy (TEM) were performed on Nicolet 6700 (Thermo Fisher Scientific, America) and HT7700 (Hitachi, Japan), respectively. The UV-vis absorption spectra were collected using a UV-6100s double beam spectrophotometer (Mapada, China).

Electrode preparation

The surface of AuE was firstly polished with 0.05 μm alumina slurry to get mirror-like and washed with ethanol and deionized water by successive ultra-sonication for 5 min.

Subsequently, the electrode was placed into an electrochemical cell using voltage cycling between − 0.3 and 1.5 V for 20 cycles in 1 M H_2SO_4 until background signal stabilization and then rinsed thoroughly with deionized water.

Preparation of 2-AET/AuE

The self-assembly of 2-AET on AuE was by dipping electrodes in 4 mM solution of 2-AET in absolute ethanol for 20 h. Following this procedure, the surface of AuE was modified with amino groups.

Preparation of MWCNTs/AuNPs/AuE

One gram of MWCNTs was treated with 80 mL of concentrated HNO_3:H_2SO_4 (3:1) (*v*/*v*) for 24 h. After ultrasonic treatment, the mixture was filtered and rinsed until the pH value reached 6.5–7.0. The treated MWCNT was dried in a vacuum oven under 120 °C for 4 h. This process was for the open of the ends of long tubes and the introduction of carboxyl groups to the surface.

MWCNTs/AuNPs were prepared by modifying a previously described procedure [34]. 4.5 mg of treated MWCNTs was added in 6.0 mL of 1.0% (*w*/*v*) sodium citrate solution to prepare a uniform suspension solution through a 5-min ultrasonic treatment. Then, this suspension was transferred to a beaker containing 75.0 mL deionized water and heated to the boiling point while stirring. Later, 750 μL of 1% (*v*/*v*) $HAuCl_4$ was rapidly added, mixed thoroughly for 5 min, and maintained at boiling point for another 5 min until the color of the solution turned into watermelon red. Finally, the resulting materials were placed in the vacuum oven to be dried under 60 °C for 2 h.

The MWCNTs/AuNPs/AuE were obtained by dropping 5 μL of MWCNT/AuNP solution containing 0.2 M NHS and 0.2 M EDC onto the surface of 2-AET/AuE for 2 h. After removal of composite materials without covalent connections by washing with PBS solution, the fabricated electrode was dried at room temperature.

Preparation of APT/MWCNTs/AuNPs/AuE and MCH/APT/MWCNTs/AuNPs/AuE

Five microliters of 5 μM thiol-labeled DNA (10 mM Tris-HCl, 1 mM EDTA, pH = 7.4) was dropwise added onto the surface of the modified electrodes and was incubated 2 h in order to make sure the immobilization of DNA with AuNPs via sulfur-gold affinity. The electrode was rinsed with Tris-HCl buffer solution to remove the physically adsorbed DNA prior to use in the following procedure. To minimize the nonspecific DNA adsorption and block the possible remaining active site on the bare gold surface, 5 μL of 1 M MCH solution was added onto APT/MWCNTs/AuNPs/AuE and incubated at 37 °C for 1 h. The fabricated APT sensor was kept at 4 °C.

Experimental detection of SM_2

The prepared aptasensor was immersed into desired concentrations of SM_2 solutions for 30 min at 37 °C and then cleaned with Tris-HCl buffer solution, followed by EIS and DPV.

The detection principle was based on the changes of the peak currents of the redox probe $[Fe(CN)_6]^{3-/4-}$ before and after the incubation of SM_2. When the background current of the aptasensor was stable, the peak current was recorded as I_0. Then, after the formation of APT-SM_2 complex, the impedance was increased, which led a decrease in peak current and recorded as I. The changes of the current response (ΔI) were given by $\Delta I = I_0 - I$. The design concept of the detection system was displayed in Scheme 2.

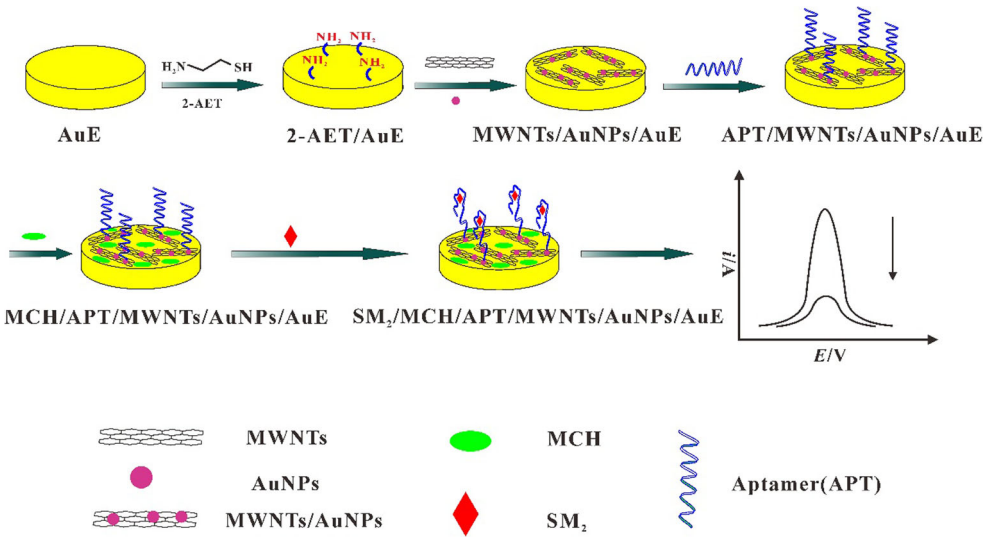

Scheme 2 Schematic diagram of the aptasensor to detect SM_2

EIS were performed under a signal amplitude of 5 mV over the frequency range of 10 kHz to 10 mHz in a 10 mM $K_4[Fe(CN)_6]/K_3[Fe(CN)_6]$ solution containing 0.1 M KCl. DPV were registered in the potential range from 0.0 to 0.5 V vs Ag/AgCl at room temperature in a 5 mM $K_4[Fe(CN)_6]/K_3[Fe(CN)_6]$ solution containing 0.1 M KCl. The parameters applied were the following: 50 mV pulse amplitude, 0.1 pulse width, and 0.5 s pulse period.

Results and discussion

Physicochemical characterization of the materials

The FTIR spectra confirmed the successful synthesis of the materials. As illustrated in Fig. 1(a), there is a peak in the FTIR spectrum of MWCNTs at 1547.52 cm^{-1}, which can be assigned to the C–C vibration. As shown in Fig. 1(b), the FTIR spectrum of carboxylic MWCNTs presents a characteristic carboxyl peak at 1711.02 cm^{-1} attributed to C=O stretching, suggesting that the carboxylic groups' introduction into MWCNTs that improve the electrical catalytic properties of MWCNTs is successful [35]. Simultaneously, the C–C vibration peak of carboxylic MWCNTs enhanced oxidation treatment, which means that some molecular structures are interrupted to form smaller structures. The same vibrational peaks of carboxylic MWCNTs appear in the spectrum of the nanocomposite with AuNPs (Fig. 1(c)), as expected.

UV-vis spectrophotometry was used to investigate the nanocomposite (Fig. 2). The spectra of the MWCNT solution show no absorption peak. For AuNPs, a sharp peak at around 520 nm appears. With the addition of AuNPs to MWCNTs, the peak at 520 nm decreased in intensity, indicating that AuNPs are successfully decorated onto the MWCNTs [30].

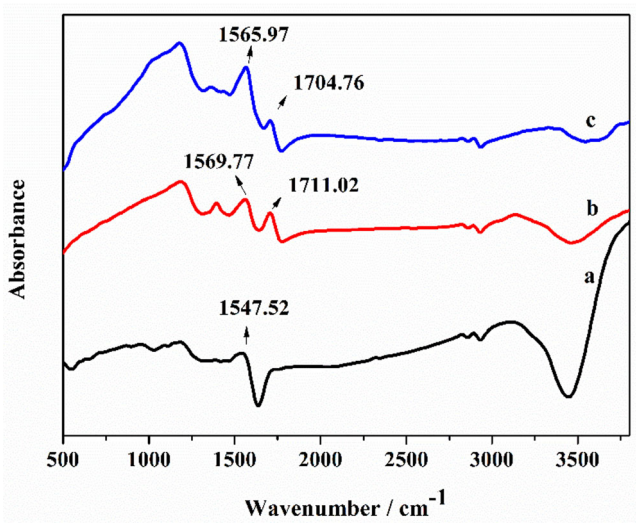

Fig. 1 FTIR spectra of (a) MWCNTs, (b) carboxylic MWCNTs, and (c) MWCNTs/AuNPs

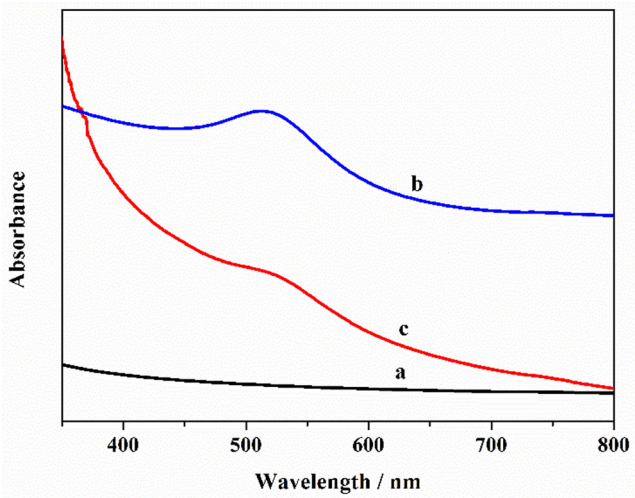

Fig. 2 UV-vis spectra of (a) MWCNTs, (b) AuNPs, and (c) MWCNTs/AuNPs

Also, we used TEM to characterize MWCNTs/AuNPs (Fig. 3). TEM image of MWCNTs (Fig. 3a) clearly shows the typical nanotube morphology. Compared to MWCNTs, the length of carboxylic MWCNTs decreases remarkably. The long tubes are split into shorter tubes, revealing an increased number of open ends, which increases the specific surface area and reactive site of the MWCNTs (Fig. 3b). In the case of MWCNTs/AuNPs, AuNPs are observed as dark dots that are well dispersed and uniformly deposited on the ends or on the sidewalls of MWCNTs (Fig. 3c). The diameter of AuNPs ranges from 10 to 20 nm. These results were consistent with the result of FTIR spectra, which were similar to those of previous studies [34].

In order to further validate the composites of MWCNTs/AuNPs, the energy-dispersive X-ray spectroscopy (EDS) elemental analysis has been operated. As expected, the signals for C and Au elements from MWCNTs and AuNPs are detected in the EDS result (Fig. 3d).

Characteristics of electrochemistry on electrode surface

EIS is an effective method to study the interface characteristics of modified electrodes. Figure 4 shows the impedance spectroscopy of the different modified electrodes, and the impedance data are fitted to an equivalent circuit, shown as an inset in Fig. 4, which includes the commonly present electrolyte resistance (Rs), electron-transfer resistance (Ret), constant phase element (Q), and Warburg impedance (Zw). As shown in Fig. 4, the bare AuE shows a relatively small semicircle domain, which is estimated to be about 48.58 Ω. In the next stage, the Ret increases obviously, which might be attributed to the fact that the formed $–NH_2$ groups hinder the electron transfer to the electrode surface (98.89 Ω). After the surface is modified by MWCNTs/AuNPs, the Ret decreases and is less

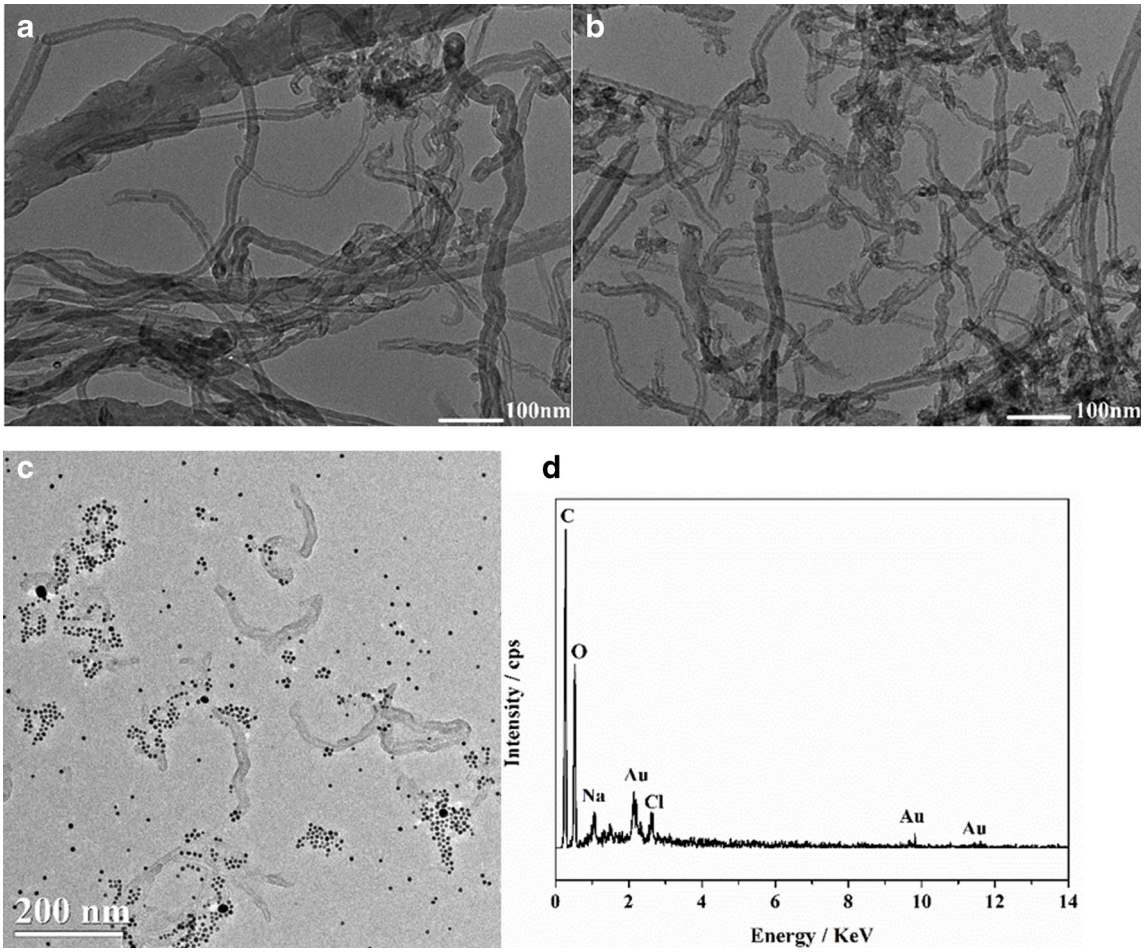

Fig. 3 TEM image of **a** MWCNTs, **b** carboxylic MWCNTs, and **c** MWCNTs/AuNPs, and **d** EDS elemental analysis spectrum of MWCNTs/AuNPs

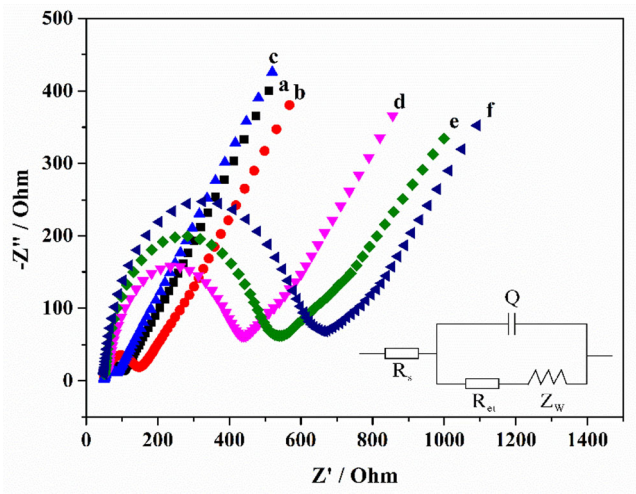

Fig. 4 EIS of the different electrodes (a) bare AuE, (b) 2-AET/AuE, (c) MWCNTs/AuNPs/AuE, (d) APT/MWCNTs/AuNPs/AuE, (e) MCH/APT/MWCNTs/AuNPs/AuE, and (f) SM_2/MCH/APT/MWCNTs/AuNPs/AuE. Supporting electrolyte, 10 mM $[Fe(CN)_6]^{3-/4-}$ + 20 mM PBS (pH 7.4) solution. The frequency range is at $1 \times 10^{-1} \times 10^5$ Hz. Inset is the equivalent circuit mold applied to fit the impedance spectra

than the bare AuE, which indicates the introduction of nanocomposite that has a high specific surface area, and a synergistic effect of MWCNTs with AuNPs can effectively increase the electrical conductivity (30.25 Ω). The value of Ret increases to 385 Ω after immobilization of APT, owing to the electrostatic repulsion between the negatively charged interface resulted by negative charge of APT and the negatively charged redox probe $[Fe(CN)_6]^{3-/4-}$. Also, a further increment in Ret (482.6 Ω) is observed after the addition of MCH is attributed to the blockage of any remaining free spaces on the electrode. When the fabricated electrode reacts with SM_2, the value of Ret increases to 593.1 Ω, due to the specific binding of SM_2 that decreases the electron transfer efficiency.

Moreover, DPV was also employed to investigate the role of composite material amplification. As shown in Fig. 5A, the two curves represent, respectively, that APT is immobilized on the bare AuE and MWCNT/AuNP-modified AuE. It is seen that the increased signal response of $[Fe(CN)_6]^{3-/4-}$ was recorded by using the immobilization interface of MWCNT/AuNP-modified AuE. The reason seems that MWCNTs/

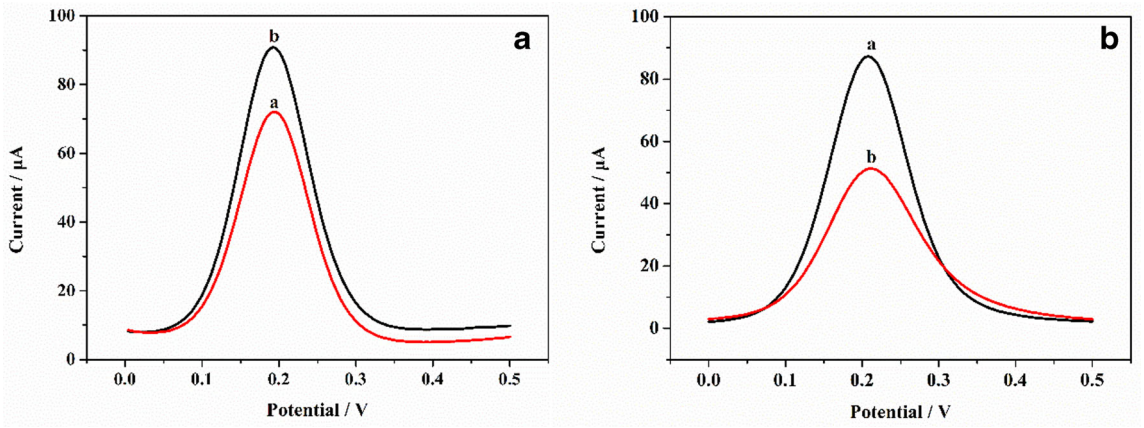

Fig. 5 **A** DPV of different electrodes in 20 mM PBS containing 5 mM $[Fe(CN)_6]^{3-/4-}$ and 0.1 M KCl: (a) MCH/APT/AuE, (b) MCH/APT/MWCNTs/AuNPs/AuE. **B** DPV of the MCH/APT/MWCNTs/AuNPs/AuE for SM_2 in the (a) absence or the (b) presence of 50 ng mL^{-1} after incubation

AuNPs can not only enhance the immobilization sites of DNA but also promote the electronic transfer. This result demonstrates that the MWCNT/AuNP-modified AuE is very useful for SM_2 sensing.

The feasibility of the proposed protocol using DPV was investigated by incubating the sensing interface with 0 and 50 ng mL^{-1} of SM_2 solution, respectively, under the same experimental conditions. As shown in Fig. 5B, when the APT-SM_2 recognition reaction was carried out, the change of the current response was calculated as 37.01 μA, which decreased by 43.6%. The results are consistent with the EIS results, indicating that this present method can be successfully used to detect SM_2.

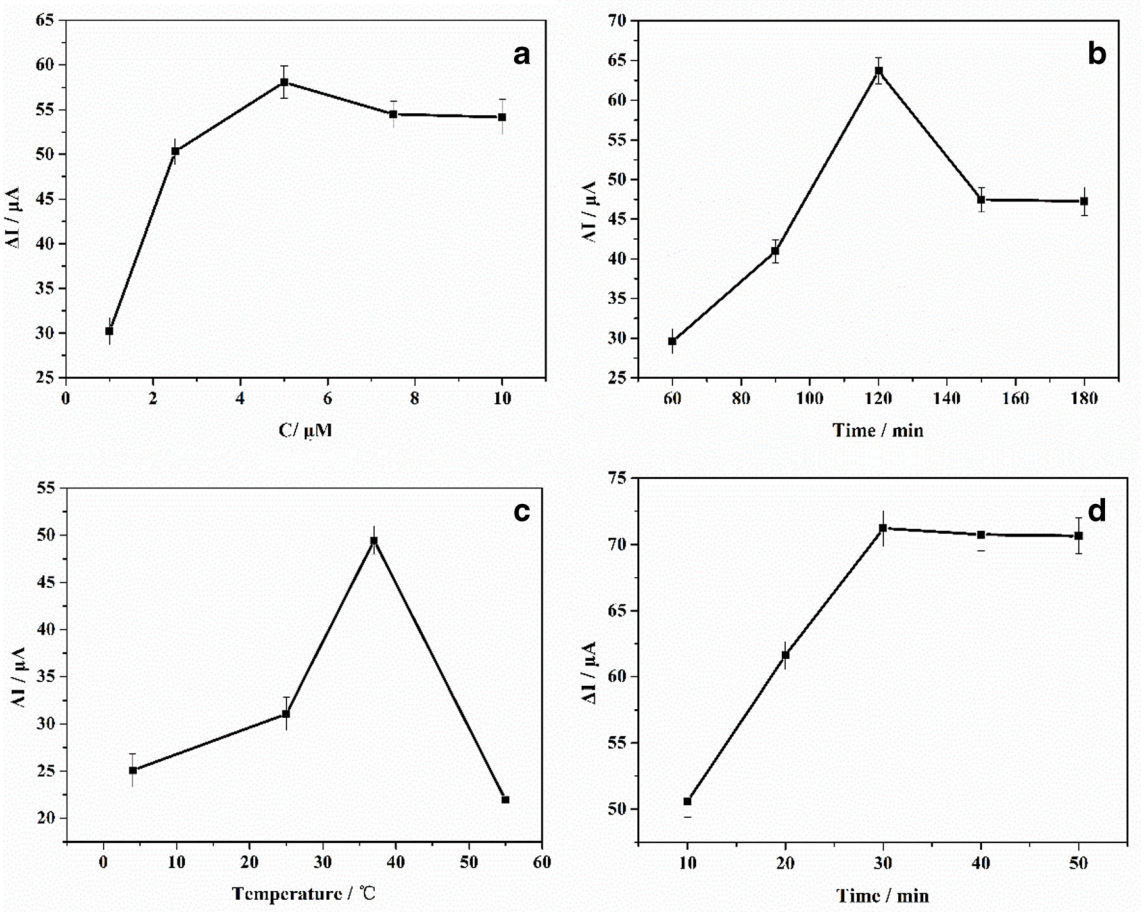

Fig. 6 Optimization of the experimental conditions: effects of **a** APT concentration, **b** APT incubation time, **c** APT incubation temperature, and **d** SM_2 interaction time. Error bars are the standard deviations of three experiments. The DPV conditions were the same as Fig. 4

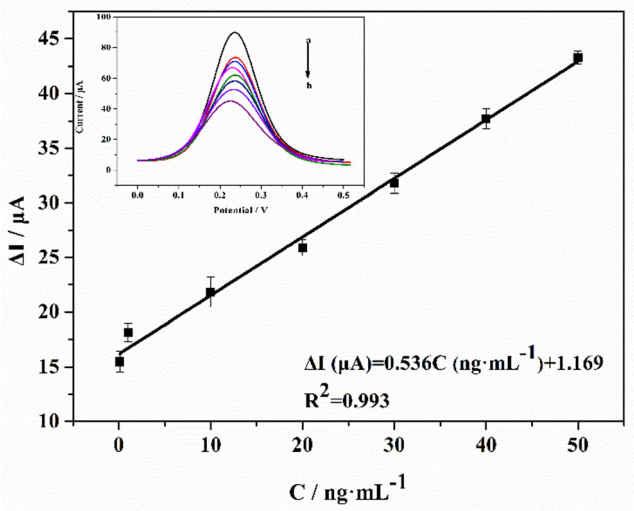

Fig. 7 Calibration curve of DPV responses for varying SM_2 concentrations from 0.1 to 50 ng mL^{-1}. Inset shows the peak currents of the electrochemical aptasensor to various concentrations of SM_2 (from (a)–(h): 0, 0.1, 1, 10, 20, 30, 40, and 50 ng mL^{-1})

Optimization of experimental conditions

To obtain a perfect sensitivity, some experimental parameters were investigated and the decrease of $[Fe(CN)_6]^{3-/4-}$ peak currents response before and after the SM_2 treatment (ΔI) was used as an indicator.

For finding the optimum concentration of APT that immobilized the electrode, five different concentrations of solution were studied (1.0, 2.5, 5.0, 7.5, and 10.0 μM). As shown in Fig. 6a, the ΔI increased rapidly with the APT concentration from 1 to 5 μM, then remained nearly constant. It was probably because the immobilization of APT had reached saturation point when the concentration of APT was more than 5.0 μM. Therefore, the concentration of 5.0 μM was selected for the preparation of the proposed aptasensor.

The incubation time of APT was investigated as it was one of the important parameters of aptasensor. It was found that ΔI increased gradually with increasing incubation time and then tended to level off after more than 120 min (Fig. 6b). This is probably owing to the full coverage of the active sites on the electrode surface by the APT that stands after 120 min. Hence, the incubation time of 120 min was applied in the subsequent work.

The influence of incubation temperature of APT was also studied over range of 4–55 °C. As shown in Fig. 6c, the ΔI increased when the temperature rose and achieved a maximum at 37 °C. Thus, the incubation temperature was optimal and chosen.

The different interaction time of SM_2 might cause the peak current decreases in different degrees. Therefore, the effect of interaction time was studied to determine the optimum condition. As shown in Fig. 6d, the ΔI increased as the interaction time increased from 10 to 30 min, and then tended to decrease slowly, indicating that the APT-SM_2 complexes were saturated on the modified AuE surface. Considering the time of analysis, 30 min was considered as the optimal interaction time.

Detection of SM_2

The detection performance of the aptasensor was evaluated by the change of peak currents after the introduction of SM_2 at a series of concentrations under the optimal conditions. Figure 7 shows the changes of current response (ΔI) were proportional to the SM_2 concentrations ranging from 0.1 to 50 ng mL^{-1} with a regression equation of the form ΔI (μA) = 0.536C (ng mL^{-1}) + 16.169 and a linear correlation of R^2 = 0.993. A limit of detection of 0.055 ng mL^{-1} was estimated according with the 3SD/m criterion, where SD was the standard deviation (n = 12) of the signals in blank PBS solution, and m was the slope of the calibration graph. The results showed that it could successfully detect the SM_2 with low detection limit and high sensitivity. The performance of the aptasensor had also been compared with other analytical systems, as shown in Table 1.

Selectivity of the aptasensor

Besides sensitivity, selectivity was also an important feature for aptasensors. Sulfamethoxazole (SMZ) and sulfadiazine

Table 1 Comparison of the analytical performance with other methods for the determination of SM_2

Method	Linear range	Limit of detection	References
Surface plasmon resonance-based biosensor	0–200 μg kg^{-1}	1.7 μg kg^{-1}	[36]
Evanescent wave immunosensor	0.17–10.73 ng mL^{-1}	0.05 ng mL^{-1}	[13]
Enzyme-linked immunoassay	0.1–5.0 μg g^{-1}	70 ng g^{-1}	[37]
Planar waveguide evanescent wave i mmunosensor	0.19–10.10 ng mL^{-1}	0.06 ng mL^{-1}	[38]
Aptasensor	0.1–50 ng mL^{-1}	0.055 ng mL^{-1}	This work

(SDZ), which belong to the SA family, were examined for their interference effects. As shown in Fig. 8, after reaction with 50 ng mL^{-1} SMZ and 50 ng mL^{-1} SDZ, respectively, the peak current decreased slightly (Fig. 8(b), (c)). In contrast, after respectively reaction with 50 ng mL^{-1} SM_2 and the mix of 50 ng mL^{-1} SM_2, 50 ng mL^{-1} SMZ, and 50 ng mL^{-1} SDZ, there was a significant response of peak current decreasing, and the current responses in the two solutions showed less than 5% difference. It was obviously exhibited that the proposed aptasensor was able to discriminate SM_2 in complex samples from its analogues.

Reproducibility and stability of the aptasensor

The reproducibility was estimated with six purposed electrodes independently fabricated by the same process. The relative standard deviation (RSD) was 3.58% in the presence 50 ng mL^{-1} SM_2. The low value of RSD demonstrated the reliability of the fabrication process. In addition, the stability of the aptasensor was studied. After 10 consecutive measurements of DPV using the same electrode, a RSD of 4.17% was acquired. The long-time stability was also investigated. The aptasensor was kept at 4 °C in the refrigerator and measured every 3–5 days. After 30 days, the current response is approximately of the 90.08% of the original value.

Application in the detection of SM_2

In order to evaluate the applicability and reliability of the developed electrochemical aptasensor in real sample, the recovery experiment of SM_2 with different concentrations was carried out. First, 0.5 g of mashed pork samples was sonicated in 1 mL ethyl acetate. Then, it was centrifuged at 5000 rpm for 10 min. Finally, the supernatant was collected and prepared for the next step. All the pork samples were assumed to be free of SM_2. SM_2 standard solutions were spiked into the real samples to prepare the SM_2 concentrations of 2, 4, and 6 ng mL^{-1}. All the experimental measurements were performed three times independently, and the results are shown in Table 2. It was seen that the recoveries and the RSD were in the range of 96~102 and 2.1~3.7%, respectively, which confirmed that the proposed aptasensor was applicable for SM_2 detection.

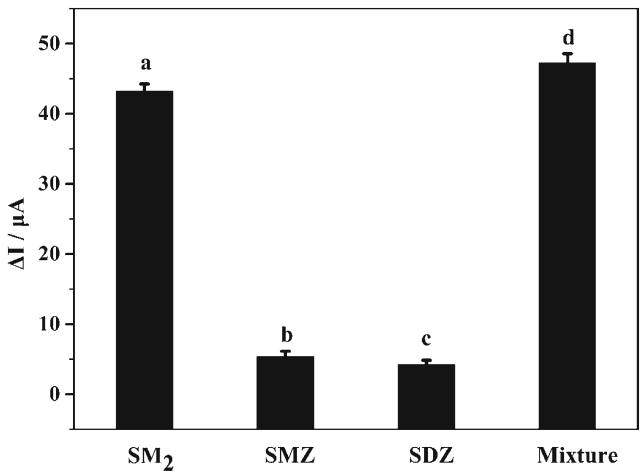

Fig. 8 Specificity of the aptasensor to 50 ng mL^{-1} SM_2 by comparing it to the different SAs at the same concentration. (a) SM_2. (b) SMZ. (c) SDZ. (d) A mix of the three SAs

Table 2 SM_2 determination in real samples by the proposed aptasensor

Samples	Added (ng mL^{-1})	Found (ng mL^{-1})	Recovery (%)	RSD
Pork samples	2	1.92	96	2.6
	4	4.08	102	3.7
	6	5.88	98	2.1

Conclusions

A novel electrochemical aptasensor based on MWCNT/AuNP-modified AuE was proposed for the determination of SM_2. The design relies on the reduction of current of $[Fe(CN)_6]^{3-/4-}$ as redox probe after APT binding to their targets and signal enhancement of nanotechnology. The experimental conditions related to APT are optimized by using DPV method and this sensor exhibits a wide linear range, low detection, admirable selectivity, and high reproducibility. Furthermore, the recovery test also demonstrates the feasibility of the constructed aptasensor for SM_2 detection in the real samples. Therefore, based on the remarkable performance, it can become a powerful tool applied in the future on-site detection.

Funding information This work was supported by the National Natural Science Foundation of China (Grant No. 61301037), Henan Science and Technology Cooperation Project (Grant No. 172106000014), Cultivation Plan for Young Core Teachers in Universities of Henan Province (No. 2017GGJS072), Foundation of Henan Educational Committee (Grant No. 13A550194), Fundamental Research Funds for the Henan Provincial Colleges and Universities (Grant No. 2014YWQQ05), and Youth Backbone Teacher Training Program of Henan University of Technology.

Compliance with ethical standards

Conflict of interest The authors declare that there is no conflict of interest.

References

1. Qiu JR, Zhao T, Liu QY, He JH, He DC, Wu GY, et al. Residual veterinary antibiotics in pig excreta after oral administration of sulfonamides. Environ Geochem Health. 2016;38:549–56.

2. Bailey C, Spielmeyer A, Hamscher G, Schuttrumpf H, Frings RM. The veterinary antibiotic journey: comparing the behaviour of sulfadiazine, sulfamethazine, sulfamethoxazole and tetracycline in cow excrement and two soils. J Soils Sediments. 2016;16:1690–704.
3. Biosic M, Mitrevski M, Babic S. Environmental behavior of sulfadiazine, sulfamethazine, and their metabolites. Environ Sci Pollut Res. 2017;24:9802–12.
4. European Commission. Regulation (EU) No 37/2010 on pharmacologically active substances and their classification regarding maximum residue limits in foodstuffs of animal origin. Off J Eur Union L. 2009;15:1–72.
5. Nebot C, Regal P, Miranda JM, Fente C, Cepeda A. Rapid method for quantification of nine sulfonamides in bovine milk using HPLC/MS/MS and without using SPE. Food Chem. 2013;141:2294–9.
6. Wu HZ, Qian MR, Wang JM, Zhang H, Ma JW, Li ZG, et al. Simultaneous determination of sulfonamides and metabolites in manure samples by one-step ultrasound/microwave-assisted solid–liquid–solid dispersive extraction and liquid chromatography–mass spectrometry. Anal Bioanal Chem. 2015;407:3545–54.
7. Kung TA, Tsai CW, Ku BC, Wang WH. A generic and rapid strategy for determining trace multiresidues of sulfonamides in aquatic products by using an improved QuEChERS method and liquid chromatography–electrospray quadrupole tandem mass spectrometry. Food Chem. 2015;175:189–96.
8. Jansomboon W, Boontanon SK, Boontanon N, Polprasert C, Da CT. Monitoring and determination of sulfonamide antibiotics (sulfamethoxydiazine, sulfamethazine, sulfamethoxazole and sulfadiazine) in imported Pangasius catfish products in Thailand using liquid chromatography coupled with tandem mass spectrometry. Food Chem. 2016;212:635–40.
9. Xia L, Liu LJ, Lv XX, Qu F, Li GL, You JM. Towards the determination of sulfonamides in meat samples: a magnetic and mesoporous metal-organic framework as an efficient sorbent for magnetic solid phase extraction combined with high-performance liquid chromatography. J Chromatogr A. 2017;1500:24–31.
10. Deng KJ, Lan XH, Sun G, Ji LY, Zheng XL. Determination of sulfonamide residues in chicken liver using high-performance liquid chromatography. Food Anal Methods. 2016;9:3337–44.
11. Summa S, Magro SL, Armentano A, Muscarella M. Development and validation of an HPLC/DAD method for the determination of 13 sulphonamides in eggs. Food Chem. 2015;187:477–84.
12. Chen C, Zhang XF, Long Z, Zhang JY, Zheng CB. Molecularly imprinted dispersive solid-phase microextraction for determination of sulfamethazine by capillary electrophoresis. Microchim Acta. 2012;178:293–9.
13. Ruiz CG, Marina ML. Recent advances in the analysis of antibiotics by capillary electrophoresis. Electrophoresis. 2006;27:266–82.
14. Ma MF, Wen K, Beier RC, Eremin SA, Li CL, Zhang SX, et al. Chemiluminescence resonance energy transfer competitive immunoassay employing hapten-functionalized quantum dots for the detection of sulfamethazine. ASC Appl Mater Interfaces. 2016;8:17745–50.
15. Liang X, Ni HJ, Beier RC, Dong YN, Li JY, Luo XS, et al. Highly broad-specific and sensitive enzyme-linked immunosorbent assay for screening sulfonamides: assay optimization and application to milk samples. Food Anal Methods. 2014;7:1992–2002.
16. Pastor-Navarro N, Gallego-Iglesias E, Maquieira A, Puchades R. Immunochemical method for sulfasalazine determination in human plasma. Anal Chim Acta. 2007;583:377–83.
17. Hao XJ, Zhou XH, Zhang Y, Long F, Song L, Shi HC. Portable and reusable optofluidics-based biosensing platform for ultrasensitive detection of sulfadimidine in dairy products. Sensors. 2015;15:8302–13.
18. Tuerk C, Gold L. Systematic evolution of ligands by exponential enrichment: RNA ligands to bacteriophage T4 DNA polymerase. Science. 1990;249:505–10.
19. Ellington AD, Szostak JW. In vitro selection of RNA molecules that bind specific ligands. Nature. 1990;346:818–22.
20. Song SP, Wang LH, Li J, Zhao JL, Fan CH. Aptamer-based biosensors. TrAC Trend Anal Chem. 2008;27:108–17.
21. Luo ZW, Wang YM, Lu XY, Chen JM, Wei FJ, Huang ZJ, et al. Fluorescent aptasensor for antibiotic detection using magnetic bead composites coated with gold nanoparticles and a nicking enzyme. Anal Chim Acta. 2017;984:177–84.
22. Wang AC, Zhao HM, Chen XC, Tan B, Zhang YB, Quan X. A colorimetric aptasensor for sulfadimethoxine detection based on peroxidase-like activity of graphene/nickel@palladium hybrids. Anal Biochem. 2017;525:92–9.
23. Chen AL, Jiang XL, Zhang WW, Chen G, Zhao Y, Tunio TM, et al. High sensitive rapid visual detection of sulfadimethoxine by label-free aptasensor. Biosens Bioelectron. 2013;42:419–25.
24. Kim YJ, Kim YS, Niazi JH, Gu MB. Electrochemical aptasensor for tetracycline detection. Bioprocess Biosyst Eng. 2010;33:31–7.
25. Liu ZY, Yuan R, Chai YQ, Zhuo Y, Hong CL, Yang X. Highly sensitive, reusable electrochemical aptasensor for adenosine. Electrochim Acta. 2009;54:6207–11.
26. Yang K, Xing BS. Desorption of polycyclic aromatic hydrocarbons from carbon nanomaterials in water. Environ Pollut. 2007;145:529–37.
27. Wei JM, Sun WL, Pan WY, Yu XQ, Sun G, Jiang H. Comparing the effects of different oxygen-containing functional groups on sulfonamides adsorption by carbon nanotubes: experiments and theoretical calculation. Chem Eng J. 2017;312:167–79.
28. Hrapovic S, Liu Y, Male KB, Luong JHT. Electrochemical biosensing platforms using platinum nanoparticles and carbon nanotubes. Anal Chem. 2004;76:1083–8.
29. Zheng TY, Bott S, Huo Q. Techniques for accurate sizing of gold nanoparticles using dynamic light scattering with particular application to chemical and biological sensing based on aggregate formation. ACS Appl Mater Interfaces. 2016;8:21585–94.
30. Magar HS, Ghica ME, Abbas MN, Brett CMA. A novel sensitive amperometric choline biosensor based on multi walled carbon nanotubes and gold nanoparticles. Talanta. 2017;167:462–9.
31. Deiminiat B, Rounaghi GH, Arbab-Zavar MH, Razavipanah I. A novel electrochemical aptasensor based on f-MWCNTs/AuNPs nanocomposite for label-free detection of bisphenol A. Sensors Actuators B Chem. 2017;242:158–66.
32. Taghdisi SM, Danesh NM, Emrani AS, Ramezani M, Abnous K. A novel electrochemical aptasensor based on single-walled carbon nanotubes, gold electrode and complimentary strand of aptamer for ultrasensitive detection of cocaine. Biosens Bioelectron. 2015;73:245–50.
33. Fei AR, Liu Q, Huan J, Qian J, Dong XY, Qiu B, et al. Label-free impedimetric aptasensor for detection of femtomole level acetamiprid using gold nanoparticles decorated multi walled carbon nanotube-reduced graphene oxide nanoribbon composites. Biosens Bioelectron. 2015;70:122–9.
34. Kangkamano T, Numnuam A, Limbut W, Kanatharana P, Thavarungkul P. Chitosan cryogel with embedded gold nanoparticles decorated multi walled carbon nanotubes modified electrode for highly sensitive flow based non-enzymatic glucose sensor. Sensors Actuators B Chem. 2017;246:854–63.

35. He BS, Zhang JX. Rapid detection of ascorbic acid based on a dual-electrode sensor system using a powder microelectrode embedded with carboxyl multi-walled carbon nanotubes. Sensors. 2017;17:1549–61.
36. Gaudin V, Pavy ML. Determination of sulfamethazine in milk by biosensor immunoassay. J AOAC Int. 1999;82:1316–20.
37. Mccaughey WJ, Elliott CT, Crooks SRH. Determination of sulphadimidine in animal feedstuffs by an enzyme-linked immunoassay. Food Addit Contam B. 1990;7:259–64.
38. Liu LH, Zhou XH, Xu WQ, Song BD, Shi HC. Highly sensitive detection of sulfadimidine in water and dairy products by means of an evanescent wave optical biosensor. RSC Adv. 2014;4:60227–33.